Available online at www.sciencedirect.com
SCIENCE DIRECT®
Environmental Modelling & Software 19 (2004) 1065–1076
Environmental Modelling & Software
www.elsevier.com/locate/envsoft

Description and verification of an aquatic optics Monte Carlo model

Manuel Gimond *

Kennedy Space Center, Dynamac Corporation, Mail Code DYN-6, FL 32899, USA

Received 1 April 2003; received in revised form 1 October 2003; accepted 3 November 2003

Abstract

An open source aquatic optics Monte Carlo (AOMC) model is described and evaluated. The open source nature of the AOMC software allows for a complete peer review process. The AOMC model simulates apparent optical properties commonly measured in aquatic systems. These include spectral or non-spectral radiance, upwelling and downwelling planar and scalar irradiances. The model output can be in a non-gridded or gridded format with the latter used to simulate a radiometric image. In gridded mode, the user may specify a bottom target whose reflecting characteristics are independent from the surrounding water bottom boundary. In both gridded and non-gridded mode, the model inputs consist of depth dependent concentrations of the various components comprising the simulated aquatic environment, their inherent optical properties, and environmental characteristics such as skylight distribution and optical properties of the aquatic bottom boundary. The model is evaluated by comparing its output to: (1) a test of the model's closure, (2) an evaluation of a known relationship, (3) the comparison with results from other published numerical models, and (4) the simulation of a spectral "pivot-point". The results of the evaluation indicate good agreement between the model and the anticipated outcome.

Keywords: Monte Carlo model; Aquatic or hydrologic optics; Radiance; Irradiance; AOMC

Software availability

Name:	Aquatic optics Monte Carlo (AOMC) model
Developer:	Manuel Gimond
Contact address:	Kennedy Space Center, Mail Code DYN-6, FL 32899, USA
Telephone, fax and e-mail:	Tel.: +1-321-867-2499; fax: +1-321-867-2502; e-mail(s): gimonm@kscems.ksc.nasa.gov or gimond@fugadeideas.org
Year first available:	2003
Program language:	FORTRAN 90
Software required:	FORTRAN 90 compiler
Hardware required:	Most computing platforms
Program size:	110 kb
Availability and cost:	Open source code available at http://aomc.fugadeideas.org or by contacting the author

1. Introduction

A scientific understanding of the interaction between electromagnetic radiation—particularly that portion of the spectrum to which the human eye is sensitive—and the aquatic medium, plays an important role in quantifying the influence of the constituents comprising the natural water body on the intensity and angular distribution of light. The radiation (light) field that results from the interaction between the external light source (e.g., sun) and the aquatic medium is important to the distribution of biological organisms such as submerged aquatic vegetation (Kirk, 1994) and fish whose vision is a source of sensory information (Pitcher, 1993). From a quantitative understanding of the interaction between light and water body constituents, one can extract information about state variables in the aquatic medium (e.g., concentrations of chlorophyll containing organisms and total suspended sediments) from in situ, airborne, or spaceborne based spectro-optical measuring devices. Because the interaction between electromagnetic radiation and the components of the aquatic medium is complex, analytical mathematical models

* Tel.: +1-321-867-2499; fax: +1-321-867-2502.
E-mail address: gimonm@kscems.ksc.nasa.gov (M. Gimond).

1364-8152/$ - see front matter © 2004 Elsevier Ltd. All rights reserved.
doi:10.1016/j.envsoft.2003.11.010

are difficult to develop and solve. This is due in part to the stochastic (probabilistic) nature of the interaction between the photons and their environment. One approach to simulating the propagation of light in an aquatic medium is through statistical simulation methods also known as Monte Carlo (MC) methods. Stochastic models are probabilistic models that trace the path of a series of photons within an attenuating medium. Results from MC models are commonly found in aquatic optics publications; however, little information is given about these models, precluding effective verification of the computational results. Kirk (1981a, b) is one of few to have published a MC model which simulates the light field resulting from a point source of light illuminating an infinitely deep water body. It has limitations in that it does not simulate an optically shallow or vertically stratified water body. This paper describes an aquatic optics Monte Carlo model (hereupon referred to as AOMC) for simulating the light field within, and just above, a water body. The AOMC model can simulate a vertically stratified water body with a finite depth whose bottom optical characteristics are defined as part of the user supplied input. The AOMC model allows the input of a realistic sky distribution and the use of separate volume scattering functions (VSF) for each water quality constituent. The model traces the paths taken by the photons in a three-dimensional environment allowing for three-dimensional radiometric output. Currently, the AOMC model assumes a waveless air–water interface and a horizontally invariant bottom depth. The open source nature of the AOMC model allows for a complete peer review process of scientific work utilizing results computed from the model.

The underlying theory is presented, followed by the description and evaluation of the AOMC model. The evaluation consists of: (1) a test of the model's closure, (2) an evaluation of a known relationship, (3) comparison with results from other published numerical models (developed using differing techniques and underlying assumptions), and (4) the simulation of a spectral "pivot-point".

2. Theory

The greatest source of light to most terrestrial aquatic systems is the sun. As light from the sun penetrates the earth's atmosphere, a fraction of its energy is absorbed and scattered, with the latter contributing to the diffuse skylight. As a result, the impinging light on the surface of a water body is composed of both direct sunlight and diffuse skylight. As the light penetrates, the air–water interface and propagates through the aquatic medium, it interacts with the constituents comprising that medium. This interaction results in two possible outcomes: absorption and scattering. The probability associated with these outcomes is determined from the inherent optical properties (IOPs) of each constituent in the aquatic medium. In mathematical models, the fraction of radiant energy absorbed by the medium is commonly expressed in terms of an absorption coefficient a. The units of a are typically m^{-1} (all symbols presented in this paper are listed in Appendix A). The coefficient a is wavelength (λ) dependent as is all subsequent terms presented in this paper (except when specified). The absorption coefficient is composed of the components comprising the aquatic medium as (Bukata et al., 1995):

$$a(\lambda) = a^*(\lambda)c, \tag{1}$$

where a^* is the specific absorption coefficient (m^2 mg^{-1}), and c is the concentration of the medium constituents (mg m^{-3}). The model assumes that the absorption coefficient is linearly related to the concentration of the entity; this has been shown to be an overly simplified assumption since identical organisms (such as phytoplankton) are known to have varying specific coefficients under different growing conditions (Fennel and Boss, 2003). For a medium, such as water, containing more than one component, Eq. (1) is composed of additive terms such as (Bukata et al., 1995):

$$a(\lambda) = a_w(\lambda) + a_1^*(\lambda)c_1 + a_2^*(\lambda)c_2 + \cdots + a_i^*(\lambda)c_i, \tag{2}$$

where a_w is the absorption coefficient of pure water (m^{-1}), and subscript i refers to the i^{th} number of the aquatic constituent.

In a similar fashion, the fraction of radiant energy scattered by the medium is commonly expressed as a scattering coefficient b in mathematical models. In the AOMC model, only elastic scattering is considered (i.e., Raman scattering and fluorescence of color dissolved organic material and other pigments are not considered). The unit of b is m^{-1}. The scattering coefficient is composed of the components comprising the medium as (Bukata et al., 1995):

$$b(\lambda) = b_w(\lambda) + b_1^*(\lambda)c_1 + b_2^*(\lambda)c_2 + \cdots + b_i^*(\lambda)c_i, \tag{3}$$

where b_w is the scattering coefficient of pure water (m^{-1}) and b_i^* is the specific scattering coefficient for the constituent i. When a photon is scattered by a constituent of a medium (such as a suspended sediment), its direction is altered. The angle of scatter is specified in terms of a VSF $\beta(\theta,\phi,\lambda)$ defined as (Petzold, 1972):

$$\beta(\theta,\phi,\lambda) = \frac{dI(\theta,\phi,\lambda)}{E_{inc}(\lambda)dV}. \tag{4}$$

The units of β are m^{-1} sr^{-1}. β describes the amount of radiation I scattered in the polar direction θ and the azimuthal direction ϕ given a source of radiant energy

E_{inc} (W m^{-2} nm^{-1}) impinging on the volume element dV. The scattering coefficient is therefore the sum of scattered radiant energy at all angles as follows:

$$b(\lambda) = 2\pi \int_0^{\pi} \beta(\theta,\lambda)\sin\theta \, d\theta, \tag{5}$$

where the term 2π is a result of the assumed symmetry about the axis of the impinging radiation which results in $\beta(\theta,\phi,\lambda)$ being constant with respect to ϕ.

A more practical form of the VSF (Bukata et al., 1995) is the volume scattering phase function (VSPF) $\tilde{\beta}(\theta,\phi,\lambda)$ defined as:

$$\tilde{\beta}(\theta,\phi,\lambda) = \frac{\beta(\theta,\phi,\lambda)}{b(\lambda)}, \tag{6}$$

which normalizes the VSF to the total scattering function thus allowing the use of a single dataset describing the angular distribution of the scattered photon in aquatic optics models. Spectral (wavelength dependent) VSF measurements are nearly non-existent due to the complex nature of such measurements. Owing to this shortcoming, the MC model described in this paper assumes a wavelength independent VSF.

The terms $a(\lambda)$ and $\beta(\theta,\phi,\lambda)$ are optical properties of a medium that are independent of the spatial distribution of the incident radiation (i.e., they are IOPs).

The light field resulting from the interaction between light and optical constituents in the aquatic medium is presented in terms of apparent optical properties (AOPs) as measured by existing spectro-optical devices. The AOPs differ from the IOPs in that they are dependent on the instantaneous illumination conditions of the aquatic medium. Typically, these field measurements consist of the following wavelength dependent quantities:

1. *Radiance* in units of W m^{-2} sr^{-1} nm^{-1}, $L(\theta,\phi,\lambda)$, at different polar (θ) and azimuth (ϕ) angles,

$$L(\theta,\phi,\lambda) = \frac{d^2F}{d\omega \; da\cos\theta}, \tag{7}$$

where F is the radiant flux (W), dω is the differential solid angle "sinθ dθ dθ", and da is the differential area on the surface of a unit sphere.

2. *Planar irradiance* for upwelling and downwelling light (E_u and E_d, respectively) whose units are typically W m^{-2} nm^{-1},

$$E_u(\lambda) = -\int_0^{2\pi}\int_{\pi/2}^{\pi} L(\theta,\phi,\lambda)\cos\theta\sin\theta \, d\theta \, d\phi \quad \text{and}$$
$$E_d(\lambda) = \int_0^{2\pi}\int_0^{\pi/2} L(\theta,\phi,\lambda)\cos\theta\sin\theta \, d\theta \, d\phi. \tag{8}$$

3. *Scalar irradiance* for upwelling and downwelling light (E_{ou} and E_{od}, respectively) whose units are typically W m^{-2} nm^{-1},

$$E_{ou}(\lambda) = \int_0^{2\pi}\int_{\pi/2}^{\pi} L(\theta,\phi,\lambda)\sin\theta \, d\theta \, d\phi \quad \text{and}$$
$$E_{od}(\lambda) = \int_0^{2\pi}\int_0^{\pi/2} L(\theta,\phi,\lambda)\sin\theta \, d\theta \, d\phi. \tag{9}$$

From the above measurable AOPs, additional quantities describing the directional characteristic of the light field are computed as follows:

$$\bar{\mu}_u(\lambda) = \frac{E_u(\lambda)}{E_{ou}(\lambda)} \quad \text{and} \quad \bar{\mu}_d(\lambda) = \frac{E_d(\lambda)}{E_{od}(\lambda)}, \tag{10}$$

where the quantities $\bar{\mu}_u$ and $\bar{\mu}_d$ are the mean cosines of the polar angle of all photons contributing to radiance distribution for the upwelling and downwelling light stream, respectively.

For a detailed derivation of these AOP quantities see Preisendorfer (1976) and Mobley (1994).

3. Description of the AOMC model

The random number generator (RNG) used in this model was originally written in F77 by Marsaglia and Zaman (1993) then later translated to FORTRAN 90 by Metcalf (2000). The FORTRAN 90 version of the aforementioned RNG is implemented in this model and has been slightly modified to use the computer system date as a seed initializer and to output a random number between 0 and 1.

The AOMC model computes the radiometric quantities $E_u(\lambda)$, $E_d(\lambda)$, $E_{ou}(\lambda)$, $E_{od}(\lambda)$, radiance at different angular directions ($L(\theta,\phi,\lambda)$), the mean cosines for the upwelling and downwelling light field ($\bar{\mu}_u(\lambda)$ and $\bar{\mu}_d(\lambda)$) and irradiance reflectance ($R(\lambda) = E_u(\lambda)/E_d(\lambda)$) at various depths within the water body as well as just above the air–water interface (see Fig. 1). The AOMC model can compute these radiometric quantities for a vertically homogeneous or heterogeneous water body. The bottom can be optically deep (i.e., deep enough so that the light reflected off of the bottom has negligible influence on the total light exiting the water body at the surface) or shallow in which case the bottom's characteristics (i.e., bottom reflectance $R_b(\lambda)$) can be specified in the model.

The input parameters required include: (1) the IOPs $a_i^*(\lambda)$, $b_i^*(\lambda)$ and $\tilde{\beta}_i$ of each constituent, (2) the environmental variables such as, (a) the concentration of the constituents, (b) skylight distribution, (c) depth of bottom and (d) wavelength dependent reflectance ($R_b(\lambda)$) characteristics of the bottom. Other input parameters required pertain to the gridding techniques used in the computation of the radiometric quantities.

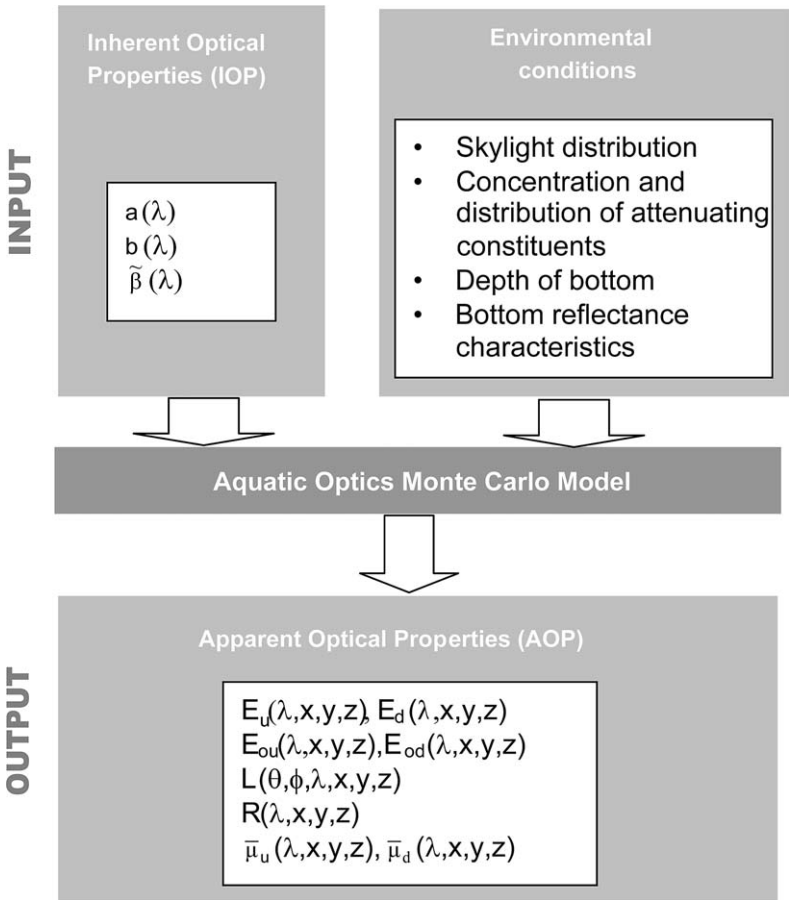

Fig. 1. Conceptual diagram showing the input parameters and output quantities for the AOMC model. Appendix A defines the symbols listed in this figure.

The IOP $a_i^*(\lambda)$ and $b_i^*(\lambda)$ for each attenuating constituent in the simulated aquatic medium are tabulated in an input file that is read by the program. The model then computes the bulk absorption and scattering coefficients for each optical layer (if the simulated medium is vertically heterogeneous) or the entire water column (if the simulated medium is vertically homogeneous) using the concentration data for each constituent (provided in a separate input file). Currently, the model does not take into account inelastic scattering such as Raman scattering that has been shown to have an important contribution to the light field for optically deep ocean waters at specific wavelengths (Stavn and Weidmann, 1992). The AOMC model allows one to define a singular VSPF $\tilde{\beta}_i$ for each constituent present in the medium. This allows the model to select the proper $\tilde{\beta}_i$ based on the constituent "i" with which the photon has a scattering event. In the current model, $\tilde{\beta}_i$ is assumed invariable across wavelength.

Skylight is the only source of light in the model. Currently, the model does not allow for the inclusion of internal light sources such as phosphorescence. The model can simulate a simple atmosphere where the sun is taken to be a single point source and the diffuse skylight is assumed evenly distributed over the upper hemisphere. The user defines the fraction of photons emitted by the sun and the diffuse skylight. Alternatively, a custom skylight distribution can be used allowing inclusion of a more realistic skylight distribution such as that measured by a radiometer or simulated by atmospheric radiative transfer models such as MODTRAN (Anderson et al., 1999). The Fresnel equations are used to determine the outcome (reflection or transmittance) of a photon's interaction at the air–water and water–air interface. If the photon is transmitted across the interface, Snell's law is used to compute the refracted angle of travel.

The bottom depth of the simulated aquatic environment is assumed parallel to the surface. The bottom reflectance characteristic is also defined by the user via an input file and specifies the probability of reflectance, $R_b(\lambda)$, at each wavelength as well as the probability of a perfectly diffuse or specular reflectance.

Another unique feature of this model is its ability to be run in a gridded or non-gridded mode. In a gridded mode (Fig. 2), the computed AOPs are calculated for

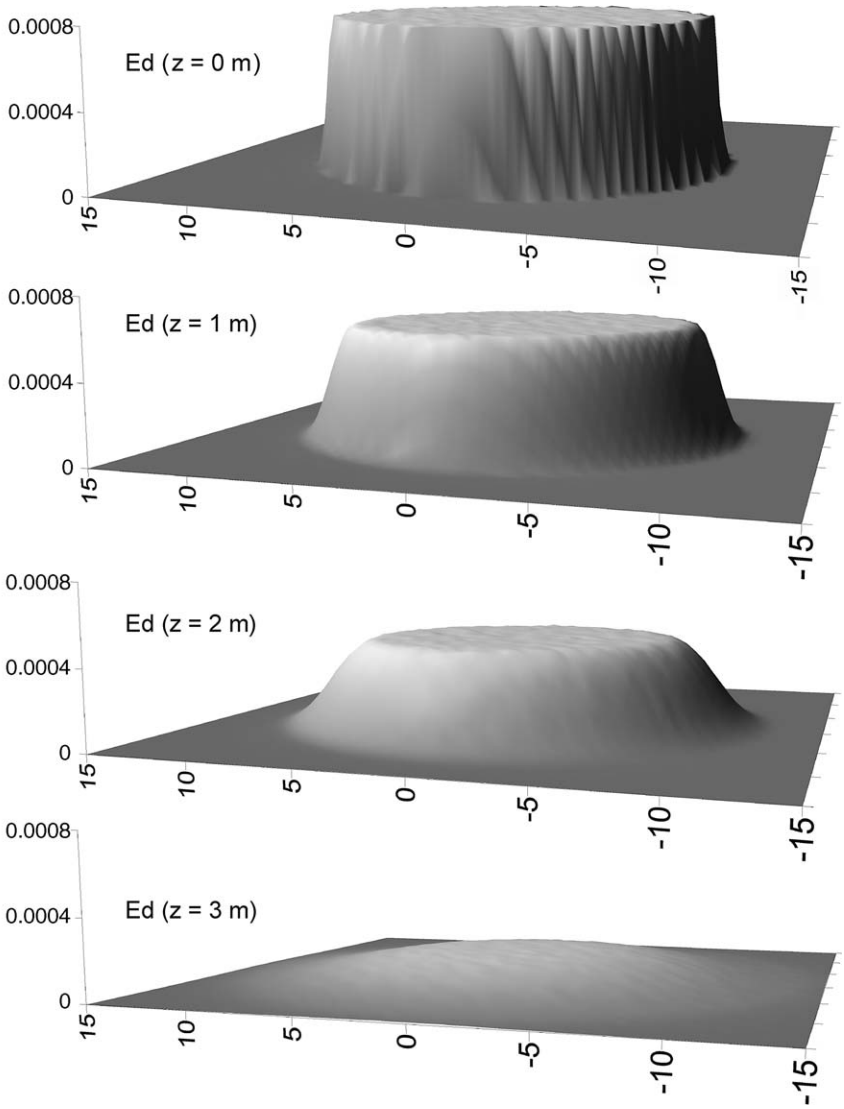

Fig. 2. AOMC output of gridded downwelling planar irradiance (E_d) at different depths z at a wavelength of 400 nm. The top figure shows a collimated beam of light with a radius of 20 units. The beam of light is attenuated and diffused as it propagates downward in the water column. The concentrations of chlorophyll and total suspended minerals used in this simulation are 0.5 mg m^{-3} and 1.0 g m^{-3}, respectively.

each discrete cell whose dimensions are specified by the user. This can be useful in computing the point-spread function (PSF) where the rate of "spreading" of light is desired. The PSF of a water body can be used to extract information about the small angle scattering phase function (Frew and Voss, 1997; Arnush, 1972). In a non-gridded mode, the model assumes that the incident light is uniformly distributed across the air–water interface and the computed AOPs are no longer horizontally dependent. If the model is run in gridded mode, the user has the option of defining a "bottom" target whose reflectance characteristic R_b is defined independently from the surrounding bottom. This option can be useful if a user wishes to evaluate the water quality conditions in which an object sitting on the bottom of the water body can be identified from surface observations (Fig. 3). Currently, only a two-dimensional rectangular shaped object or "target" can be simulated.

In addition to the horizontal gridding scheme, the model allows the user to specify a uniform vertical space interval (Fig. 4). These intervals define the location of the horizontal recording layer where the radiometric quantities (the AOPs) are to be computed. The recording layer interfaces are independent of the boundary layers defining the change in concentration of the attenuating constituents.

Two important parameters that must be defined in the AOMC model are the dimensions and the number of directional quads or bins used to log the angular direction traveled by the photon when it crosses a recording layer interface. The distribution of the quads

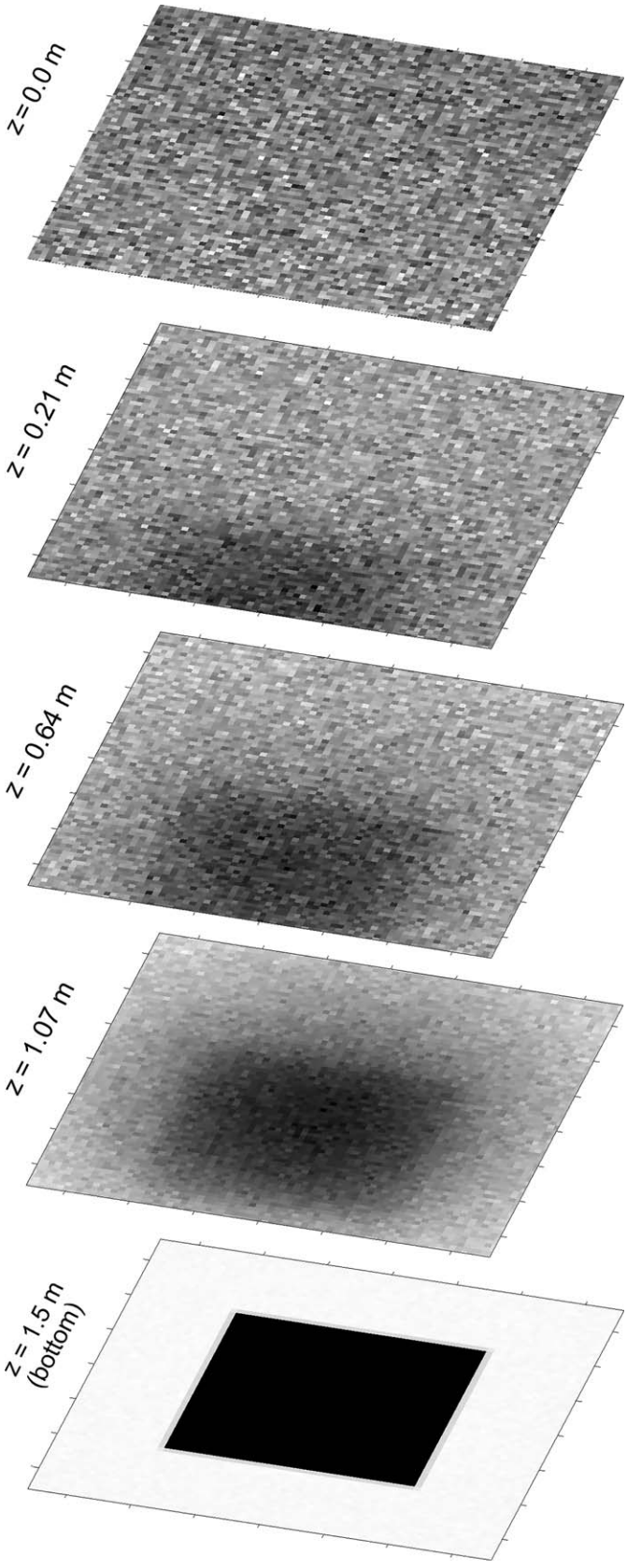

Fig. 3. Simulation of upwelling planar irradiance (E_u) at 400 nm at different depths for a bottom with a perfectly absorbing square target ($R_b^{target} = 0$). The surrounding bottom is a 20% Lambertian (80% specular) reflector with $R_b = 1.0$. The total absorption and scattering coefficients of the water column are 0.0115 and 0.006 m^{-1}, respectively. The skylight distribution data used was computed from MODTRAN 4.0 (Anderson, 1999) for a clear sky with a solar zenith angle of 20°. The shift in the location of the "footprint" of the target at decreasing depths is attributed to the angular component of the sun and the specular characteristic of the surrounding bottom.

result in a unit sphere about the point where the photon crosses the recording layer interface (Fig. 5). The number of quads used in the polar and azimuthal directions are independently defined. A polar cap (Fig. 5) is used to record the photons traveling in a near nadir direction.

If $N(\theta,\phi,k)$ represents the total number of logged photons crossing layer "k" (see Fig. 4) and traveling in the binned direction (θ,ϕ), then, at the end of a simulation, $N(\theta,\phi,k)$ is used to calculate the radiometric quantities. A fundamental concept in remote sensing is the radiant flux Φ which is defined as the flow of energy per unit time:

$$\Phi = \frac{dQ}{dt}, \tag{11}$$

where Q is the radiant energy with units of J. The radiant flux, Φ, has units of W (J s^{-1}). The energy of a single photon Q_p is defined as:

$$Q_p = h_p \upsilon, \tag{12}$$

where h_p is Planck's constant (J s) and υ is the frequency (s^{-1}) associated with the photon. When radiometric measurements are made in the field, the sensor collects or "integrates over a time interval" a large number of photons. The photons "hitting" the sensor are converted to a measurable energy via the "photo-electric effect" which is then converted to a radiometric value. The tallied events from the AOMC model cannot be independently converted to a radiometric quantity. The tallied results at each recording layer interface are only meaningful if they are normalized to the original number of photons entering the system. Hence, the tallied events at each interface are normalized to the initial number of photons. The resulting value at each interface represents the fractional value of an initialized quantity (defined at the air–water interface). The radiant flux (Φ) is proportional to the number of photons ($N(\theta,\phi,k)$) recorded at each depth interval. Using this simplistic analogy, the AOPs can then be calculated (Table 1).

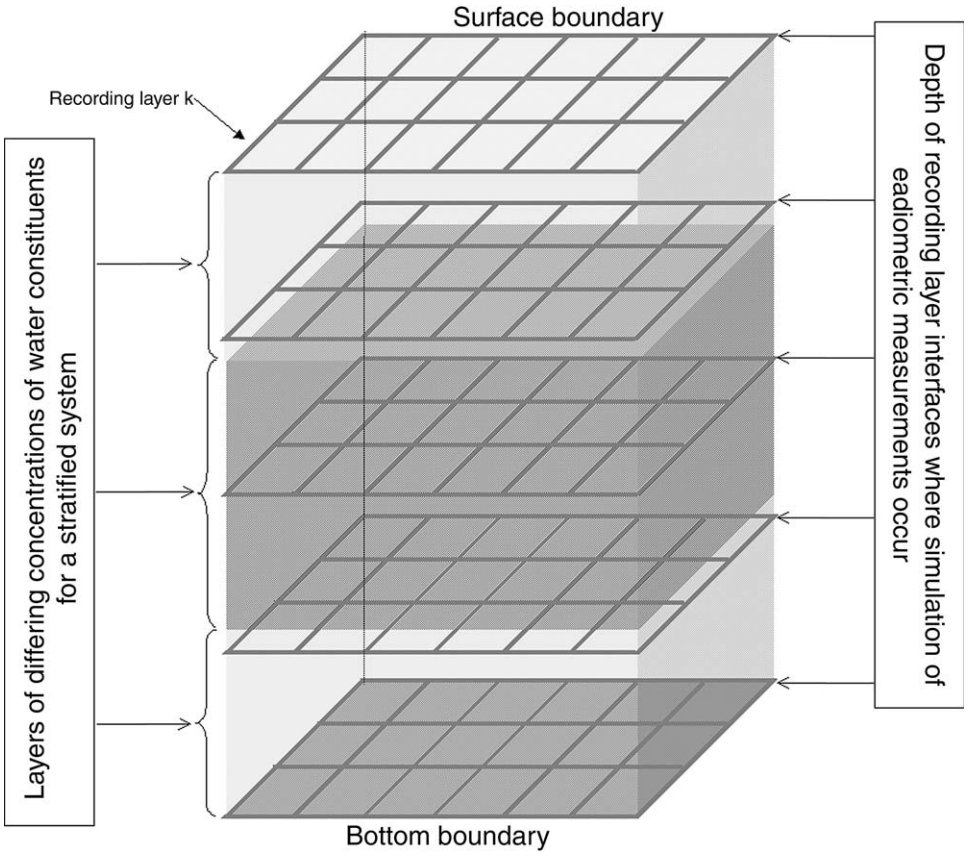

Fig. 4. Description of the different layering system used in setting up the model simulation. The model divides the water body into vertically heterogeneous layers of differing composition of water constituents (shown as shaded objects in figure). It also divides the water body into equal intervals of recording or tallying layer interfaces (shown as horizontal grids) where the simulated radiometric quantities are computed.

4. Simulation problems and results

4.1. Problem 1: a simple test for model closure

In this problem, a simple homogeneous water body with a solely absorbing (a= 1 m^{-1}) environment is simulated. The light source is a single point in the sky with a zenith angle θ_z of 60° resulting in a (below water) refracted angle θ of 40.5°. The bottom boundary is at a depth of 1 m and has a perfectly specular reflecting bottom with $R_b = 1.0$. This simulated environment prevents the ray of light from diffusing in the aquatic medium, allowing for an analytical solution of the rate of attenuation of the beam of light in the downward and upward directions. In the absence of scattering, the following equation can be used to calculate $E_d(z)$, knowing $E_d(z - dz)$ and the rate of vertical attenuation of E_d, *as*:

$$E_d(z) = E_d(z - dz)\ e^{(-k_{E_d} dz/\cos\theta)}. \quad (13)$$

Since the model computes E_d at different depths, Eq. (13) can be solved for k_{E_d}:

$$k_{E_d} = -\ln\left(\frac{E_d(z)}{E_d(z - dz)}\right)\frac{\cos\theta}{dz}. \quad (14)$$

The same reasoning can be applied to the computation of the upwelling planar irradiance attenuation coefficient k_{E_u}:

$$k_{E_u} = \ln\left(\frac{E_u(z)}{E_u(z - dz)}\right)\frac{\cos\theta}{dz}. \quad (15)$$

For this simulation, the only attenuating factor is a, therefore it is expected that $k_{E_d} = k_{E_u} = a$ for both the upwelling and downwelling light stream. As expected, using Eq. (15) in conjunction with the values of E_d computed in the model, k_{E_d} and k_{E_u} were found to be 1 indicating proper tallying and accountability for the simulated photons in the AOMC model (Table 2).

4.2. Problem 2: a simple relationship

A widely published relationship between irradiance reflectance (just beneath the air–water interface) and the IOPs a and b is expressed as (Gordon et al., 1975; Morel and Prieur, 1977; Kirk, 1981b; Sathyendranath and Platt, 1997):

$$R = r_p \frac{b_b}{a}, \quad (16)$$

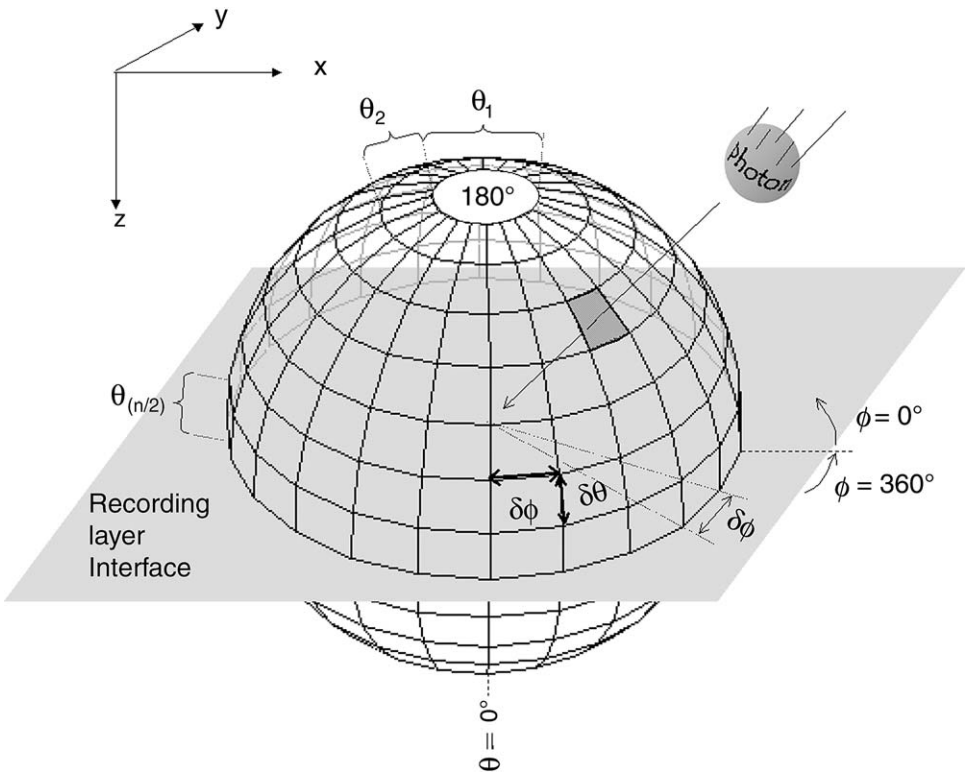

Fig. 5. Partitioning of the unit sphere into quads for use in discretizing the angular direction of travel of each photon.

where r_p is a dimensionless parameter and $b_b = bB$ (where B represents the fraction of light scattered in the backward direction and is directly calculated from the VSPF). The relationship in Eq. (16) is valid only for optically deep waters whose backscattering coefficient is much less than the absorption coefficient (Morel and Prieur, 1977). Typical values of r_p range between 0.3244 and 0.343 (Table 3). The AOMC model is run using eight different scattering coefficients ranging from 0 to 30 m^{-1}. The average of Petzold's (1972) three San Diego Harbor VSPFs is used for these simulations. The averaged VSPF results in a B value of 0.019. The absorption coefficient is fixed at 1 m^{-1} yielding a range of b_b/a ratio values between 0 and

Table 1
List of radiometric quantities and their computation in the AOMC model. The quantity $N(\theta,\phi)$ is the number of photons tallied at each recording layer interface traveling in zenith and azimuth angles θ and ϕ

Radiometric quantity	Conventional definition	Derivation from the AOMC model
Field radiance at a point in a surface (L)	$\frac{d^2\Phi}{dA\cos(\theta)\, d\theta\, d\phi}$	$\frac{N(\theta,\phi)}{\sin(\theta)\cos(\theta)\, d\theta\, d\phi}$
Downwelling planar irradiance (E_d)	$\int_0^{2\pi}\int_0^{\pi/2} L(\theta,\phi)\cos\theta\sin\theta\, d\theta\, d\phi$	$\int_0^{2\pi}\int_0^{\pi/2} N(\theta,\phi)$
Upwelling planar irradiance (E_u)	$-\int_0^{2\pi}\int_{\pi/2}^{\pi} L(\theta,\phi)\cos\theta\sin\theta\, d\theta\, d\phi$	$\int_0^{2\pi}\int_{\pi/2}^{\pi} N(\theta,\phi)$
Downwelling scalar irradiance (E_{od})	$\int_0^{2\pi}\int_0^{\pi/2} L(\theta,\phi)\sin\theta\, d\theta\, d\phi$	$\int_0^{2\pi}\int_0^{\pi/2} \frac{N(\theta,\phi)}{\cos(\theta)}$
Upwelling scalar irradiance (E_{ou})	$\int_0^{2\pi}\int_{\pi/2}^{\pi} L(\theta,\phi)\sin\theta\, d\theta\, d\phi$	$-\int_0^{2\pi}\int_{\pi/2}^{\pi} \frac{N(\theta,\phi)}{\cos(\theta)}$

Table 2
Results from model closure test. The computed attenuation coefficients (k_{E_d} and k_{E_u}) for a non-scattering medium match the input value of a (absorption coefficient) as expected

Attenuation coefficient	Expected value	Calculated from AOMC simulation
k_{E_d}	1.0	0.999
k_{E_u}	1.0	1.000

Table 3
Comparison between the coefficent r_p relating the subsurface reflectance R with the IOPs for a nadir solar angle. There is good agreement between the AOMC result and that of various authors computed using different techniques

Author(s)	r_p
Gordon et al. (1975)	0.3244
Morel and Prieur (1977)	0.33
Kirk (1981b)	0.328
Sathyendranath and Platt (1997)	0.343
AOMC	0.329

0.57. The light source is assumed 100% collimated at a sun zenith angle of 0°. The resulting reflectance values are then plotted against the b_b/a ratios and a regression (with intercept 0) is fitted to the data with the slope taken to be the coefficient r_p (Fig. 6). The resulting coefficient (r_p) of 0.3299 is in very good agreement with the published results (Table 3).

4.3. Problem 3: Mobley et al.'s (1993) canonical problems

The most comprehensive published model–model comparison in aquatic optics to date involves seven different models which were developed using different numerical techniques and assumptions (Mobley et al., 1993). Mobley et al. (1993) developed several canonical problems that differed in the depth and optical characteristics of the aquatic medium. Subsets of these problems (problems 1, 2, 3 and 6) are compared with the AOMC model.

Mobley et al.'s (1993) first problem uses a Rayleigh scattering phase function to describe the angular scattering properties of the water. The simulated water body is assumed optically deep and the sun's zenith angle is 60° with an impinging surface planar irradiance of 0.5 W m^{-2} nm^{-1}. A single wavelength is assumed for this and all subsequent problems. Two different scattering to absorption ratios are used for this problem: 0.25/1.0 and 9.0/1.0. These ratios result in a scattering albedo ω ($\omega = b/(b+a)$) of 0.2 and 0.9, as

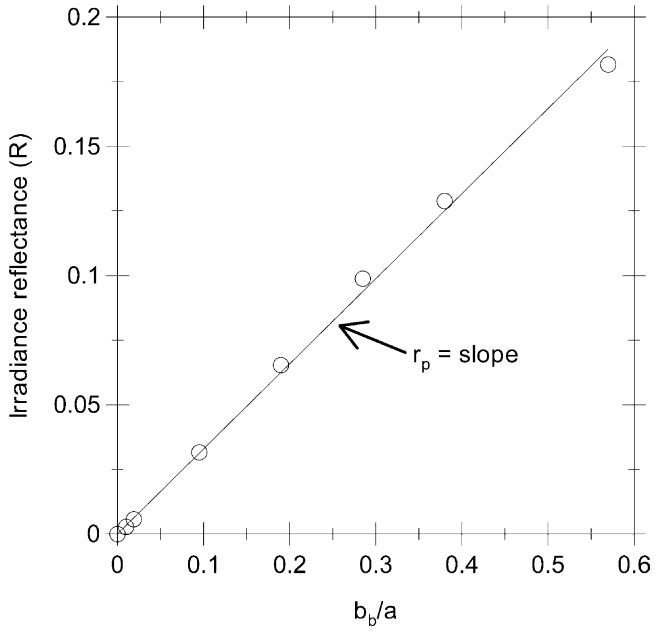

Fig. 6. Plot of modeled reflectance for eight different values of b_b/a ratios. A linear regression was fitted to these data points. The resulting slope is taken to be the coefficient r_p relating the irradiance reflectance to the IOPs b and a.

presented in Mobley et al.'s (1993) paper. Mobley et al. (1993) present the results of the model comparisons as a coefficient of variance CV:

$$\mathrm{CV} = \frac{\text{standard deviation}}{\text{sample mean}}. \tag{17}$$

The results from the AOMC model are presented and compared to those presented in Mobley et al.'s (1993) paper using the relative difference (RD) whose value is computed as:

$$\mathrm{RD} = \frac{X_{\text{Mobley et al.}} - X_{\text{AOMC}}}{X_{\text{Mobley et al.}}}, \tag{18}$$

where $X_{\text{Mobley et al.}}$ is the mean value from the models presented in Mobley et al. (1993) and X_{AOMC} is the value computed from the AOMC model. The purpose of running the simulation with this first problem is to: (1) test the model's ability to properly tally the photons at different depths, and (2) to test the scattering scheme implemented in the AOMC model. For the most part, the RD values (Table 4) fall within the published CV values for this first problem indicating good agreement between the AOMC model and Mobley et al.'s suite of models. The slight increase in error as a function of depth is expected since fewer photons find their way down the water column, thereby increasing stochastic noise in measurements computed at greater depths.

Mobley et al.'s (1993) "problem 2" substitutes the Rayleigh VSF with a VSF typical of waters with high particulate matter (Petzold, 1972). This results in a strong forward component to the VSF leading to a probability of forward scatter of 98%. The AOMC model is run only for the case where $\omega = 0.9$ since differences between models are more likely to occur with higher scattering. Once again, the agreement between this model and Mobley et al.'s model simulations is very good (Table 4) based on the low RD to CV ratio (indicating that the AOMC model output falls within the range of outputs from Mobley et al.'s model suite).

Radiance $L(\theta)$ values between the AOMC model and Mobley et al.'s model suite at various polar angles along the vertical solar plane at two different optical depths ($\tau = 0$ and $\tau = 20$) are compared (Fig. 7). The polar angle of 0° represents the direction in which the photons are traveling straight down—hence simulating the amount of light energy received by a photo-sensitive detector looking up—and the polar angle of 180° represents the direction in which the photons are traveling upward (towards the air–water interface). The agreement in $L(\theta)$ between both models is quite good.

Mobley et al.'s (1993) "problem 3" simulates a stratified water body where the concentrations of total particulate matter vary as a function of depth. This problem tests the AOMC model's ability to adjust the photon's pathlength as a function of the varying concentration of total particulate matter. Mobley et al.

Table 4
Comparison between values computed by the AOMC model and those from Mobley et al.'s (1993) suite of models for a subset of Mobley et al.'s canonical problems. The results between the AOMC model and the mean of Mobley et al.'s models (Mob.) are shown. The coefficient of variance from Mobley et al.'s models and the RD between the AOMC model and the mean values from Mobley et al.'s models are also shown

Optical depth	E_d				E_{ou}				L_u			
	AOMC	Mob.	CV	RD	AOMC	Mob.	CV	RD	AOMC	Mob.	CV	RD
Mobley et al.'s problem 1: ω= 0.2												
1	1.41–1	1.41–1	0.001	0.000	01.33–2	1.34–2	0.003	0.007	1.67–03	1.72–3	0.044	0.029
5	1.07–3	1.07–3	0.005	0.000	0.97–4	1.00–4	0.039	0.030	1.29–05	1.37–5	0.288	0.058
Mobley et al.'s problem 1: ω= 0.9												
1	3.66–01	3.66–1	0.002	0.000	3.72–1	3.72–1	0.005	0.000	4.69–2	4.85–2	0.015	0.033
5	4.33–02	4.33–2	0.003	0.000	4.35–2	4.35–2	0.007	0.000	5.75–3	5.59–3	0.052	0.028
10	3.16–03	3.16–3	0.015	0.000	3.15–3	3.20–3	0.038	0.016	4.26–4	4.37–4	0.091	0.025
Mobley et al.'s problem 2: ω= 0.9												
1	4.14–1	4.13–1	0.001	0.002	9.16–2	9.31–2	0.021	0.016	6.80–3	6.99–3	0.063	0.028
5	1.88–1	1.87–1	0.005	0.005	4.57–2	4.63–2	0.017	0.013	3.12–3	3.26–3	0.055	0.043
10	6.94–2	6.85–2	0.010	0.013	1.63–2	1.65–2	0.014	0.012	1.16–3	1.21–3	0.109	0.041
Mobley et al.'s problem 3: ω= 0.9												
Physical depth												
5 m	2.35–1	2.30–1	0.006	0.022	4.35–2	4.34–2	0.025	0.002	3.01–3	3.13–3	0.054	0.040
25 m	1.74–3	1.62–3	0.028	0.074	3.04–4	2.86–4	0.038	0.063	2.20–5	2.12–5	0.061	0.038
60 m	5.40–5	5.23–5	0.071	0.032	0.06–4	5.13–6	0.036	0.169	4.00–7	3.57–7	0.434	0.120
Mobley et al.'s problem 6: ω= 0.9												
1	1.62–1	1.62–1	0.000	0.000	9.60–4	9.81–4	0.010	0.021	7.25–5	6.84–5	0.020	0.059
5	2.29–3	2.28–3	0.003	0.004	2.28–3	2.28–3	0.002	0.000	3.60–4	3.60–4	0.010	0.000

(1993) use an analytical equation to describe the vertical profile of the IOPs. For this simulation, tabulated values of a and b are calculated from the analytical equations at 0.5 m intervals. The AOMC model simulation's results and the mean values from Mobley et al.'s model simulations are in reasonably good agreement at the 5 m depth (Table 4), but diverge at increasing depth where a RD value for E_{ou} as high as 16.9% is found at a depth of 60 m (Table 4). This divergence in simulated values can be explained by the interval resolution used to represent the vertical profile of the IOPs. Since information on the interval resolution used for the concentrations of particulate matter in the simulations presented in Mobley et al. (1993) is not available, results from the AOMC simulation presented here (Table 4) are those for a 0.5 m vertical distribution interval of IOPs.

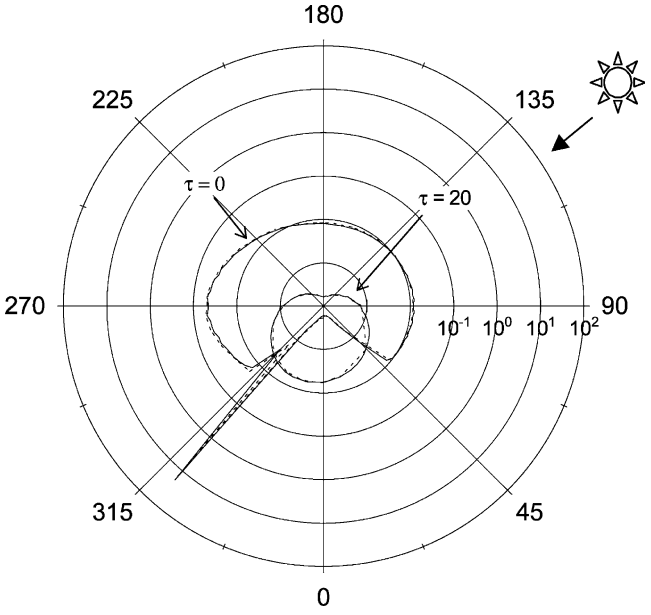

Fig. 7. Distribution of radiance (in W m^{-2} sr^{-1} nm^{-1}) for the AOMC model (solid curves) and Mobley et al.'s (1993) DO and II models (dashed curves). These values were computed from simulations using Mobley et al.'s canonical problem number 2 (with ω= 0.9). The radiance values shown are plotted at various polar angles along the sun's vertical plane. The polar angle of 0° shows the radiance value as measured by an instrument looking up (measuring downward traveling light). The polar angle of 180° shows the radiance values as measured by an instrument looking down (measuring upward traveling light).

Mobley et al.'s (1993) "problem 6" simulates an optically homogeneous water body with a finite bottom depth. The bottom is a Lambertian reflector with an irradiance reflectance of 0.5. This problem tests the AOMC model's photon interaction with a bottom boundary. The RDs for E_d and E_{ou} between the AOMC model and Mobley et al.'s models fall within Mobley et al.'s CV with the exception of the near surface values of E_{ou} and L_u (Table 4). These differences could be a result of stochastic noise—an outcome of the low number of upward traveling photons making their way toward the air–water interface. Another cause for the error is the possible difference in bin sizes used in logging the angular direction of travel of the photon at each recording depth.

4.4. Problem 4: simulation of a spectral pivot point

Natural waters contain various constituents with differing IOPs. It is this difference that allows each constituent within a water body to acquire a unique radiometric spectral signature (such as spectral surface irradiance reflectance). The spectral signature varies as a function of concentration of the constituent. However, Bukata et al. (1995) show how, for a two-component water body (water and chlorophyll), there exists a wavelength at which the bulk subsurface irradiance reflectance R is independent of chlorophyll concentration. This feature is called a pivot point. Using an analytical equation derived from the theory of light propagation through a medium (also referred to as the radiative transfer theory), they identify the pivot point feature at around 497 nm. Using the wavelength dependent specific absorption and scattering coefficients for water ($a^*_{\text{water}}(\lambda)$ and $b^*_{\text{water}}(\lambda)$, respectively) and chlorophyll ($a^*_{\text{chl}}(\lambda)$ and $b^*_{\text{chl}}(\lambda)$, respectively) from Bukata et al. (1995), and the Rayleigh and Petzold's (1972) particulate VSPF for the water and chlorophyll components, respectively, spectral irradiance reflectance signatures just beneath the air–water interface were generated for concentrations of chlorophyll of 0.0, 0.5, 1.0, 10.0 and 20.0 mg m^{-3}.

The purpose of this simulation is to evaluate the model's ability to generate realistic spectral signatures and to properly assign a probability of interaction between the photon and the two components (i.e., the ability to discriminate between a scattering event for water or chlorophyll thereby identifying which VSPF to use). Fig. 8 shows the result of these simulations and the resulting pivot point feature. This simulation shows a pivot point at around 495 nm which is in very close agreement to Bukata et al.'s (1995) value of 497 nm.

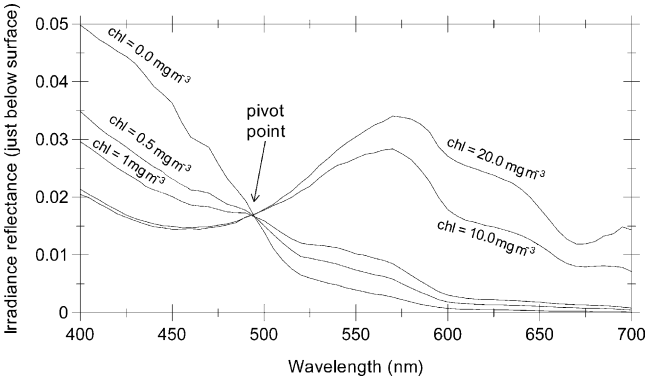

Fig. 8. MC model simulation of subsurface irradiance reflectance (R) between the wavelengths of 400 and 700 nm. The simulation is for a two-component water body: water and chlorophyll. The concentrations of chlorophyll vary between 0.0 and 20.0 mg m^{-3}. The "pivot point" (wavelength where the concentration of chlorophyll does not change the value of R) appears at around 495 nm.

5. Conclusions

An AOMC model was evaluated by (1) successfully testing for model closure, (2) reproducing a well know relationship, (3) successfully reproducing results generated from other numerical models, and (4) properly simulating and identifying the location of a "pivot point" in hyperspectral mode. These tests, or simulations, show good agreement between the AOMC model and expected results attesting to the model's reliability in simulating the light field for relatively complex water bodies. The AOMC model does make some simplifying assumptions. Currently, the AOMC model does not incorporate surface wave effects or heterogeneous bottom depths (which can be important contributors to the resulting light field under certain conditions) nor does it account for inelastic scattering (e.g., Raman scattering and fluorescence of color dissolved organic material and other pigments). The open source feature of this model makes it well suited for adaptation to various problems in various fields such as medical imaging and atmospheric sciences. The verification results presented in this paper are not to be confused with validation of the model which entail reliable simultaneous measurements of IOPs and AOPs. Such complete sets of measurements are rare and very difficult to make, particularly scattering and VSF.

Acknowledgements

The author would like to thank Paul Schmalzer, Ron Schaub and Carlton Hall for their helpful suggestions and comments. Many thanks to Emmanuel Boss and two anonymous reviewers who provided extensive comments that helped improve this paper.

Appendix A. List of frequently used symbols

Symbol	Name	Typical units
$\beta(\theta,\phi,\lambda)$	Volume scattering function	m^{-1} sr^{-1}
$\tilde{\beta}(\theta,\phi^s,\lambda)$	Volume scattering phase function	sr^{-1}
ϕ	Photon's azimuth angle of propagation	Degrees
λ	Wavelength	nm
$\bar{\mu}_d$	Downwelling mean cosine	Dimensionless
$\bar{\mu}_u$	Upwelling mean cosine	Dimensionless
θ	Photon's polar angle of propagation	Degrees
$\tau(\lambda)$	Optical depth ($\tau = \int_0^z c(z)\,dz$)	Dimensionless
ω	Scattering albedo $=b/(a+b)$	Dimensionless
$a(\lambda)$	Bulk absorption coefficient	m^{-1}
$a^*_i(\lambda)$	Specific absorption coefficient for constituent i	m^2 mg^{-1}
$b(\lambda)$	Bulk elastic scattering coefficient	m^{-1}
$b^*_i(\lambda)$	Specific scattering coefficient for constituent i	m^2 mg^{-1}
$b_b(\lambda)$	Bulk backscattering coefficient	m^{-1}

$c(\lambda)$	Bulk attenuation coefficient ($c=a+b$)	m^{-1}
$E_d(\lambda)$	Downwelling planar irradiance	W m^{-2} nm^{-1}
$E_{od}(\lambda)$	Downwelling scalar irradiance	W m^{-2} nm^{-1}
$E_{ou}(\lambda)$	Upwelling scalar irradiance	W m^{-2} nm^{-1}
$E_u(\lambda)$	Upwelling planar irradiance	W m^{-2} nm^{-1}
$F(\lambda)$, $\Phi(\lambda)$	Radiant flux	W nm^{-1}
$L(\theta,\phi,\lambda)$	Radiance	W m^{-2} sr^{-1} nm^{-1}
$L_{0^\circ}(\theta,\phi,\lambda)$	Downwelling radiance	W m^{-2} sr^{-1} nm^{-1}
$L_{180^\circ}(\theta,\phi,\lambda)$	Upwelling radiance as measured by a nadir-viewing radiometer	W m^{-2} sr^{-1} nm^{-1}
$R(\lambda)$	Irradiance reflectance $= E_u/E_d$	Dimensionless
$R_b(\lambda)$	Bottom reflectance	Dimensionless

References

Anderson, G.P., Berk, A., Acharya, P.K., Matthew, M.W., Bernstein, L.S., Chetwynd, J.H., Dothe, H., Adler-Golden, S.M., Ratlowski, A.J., Felde, G.W., Gardner, J.A., Hoke, M.L., Richtsmeier, S.C., Jeong, L.S., 1999. MODTRAN4 version 2: radiative transfer. In: Shen, S.S., Descour, M.R. (Eds.), Proceedings of the SPIE. Algorithms for Multispectral, Hyperspectral, and Ultraspectral Imagery VII, vol. 4381, pp. 455–459.

Arnush, D., 1972. Underwater light-beam propagation in the small-angle-scattering approximation. Journal of the Optical Society of America 62 (9), 1109–1111.

Bukata, R.P., Jerome, J.H., Kondratyev, K.Y., Pozdynyakov, D.V., 1995. Optical Properties and Remote Sensing of Inland And Coastal Waters. CRC Press, New York, (362 pp).

Fennel, K., Boss, E., 2003. Subsurface maxima of phytoplankton and chlorophyll: steady-state solutions from a simple model. Limnology and Oceanography 48 (4), 1521–1534.

Frew, B.J., Voss, L.J., 1997. Measurement of the point-spread function in a layered system. Applied Optics 36 (15), 3335–3337.

Gordon, H.R., Brown, O.B., Jacobs, M.M., 1975. Computed relationships between the inherent and apparent optical properties of a flat, homogeneous ocean. Applied Optics 14, 417–427.

Kirk, J.T.O., 1981a. Monte Carlo procedure for simulating the penetration of light into natural waters. CSIRO Division of Plant Industry Tech. Paper No. 36, Australia (16 pp.)

Kirk, J.T.O., 1981b. Monte Carlo study of the nature of the underwater light field in, and the relationships between optical properties of, turbid yellow waters. Australian Journal of Marine Freshwater Research 32, 517–532.

Kirk, J.T.O., 1994. Light and Photosynthesis in Aquatic Ecosystem. Cambridge University Press, Cambridge, UK, (509 pp).

Metcalf, M., 2000. Re: KISS random number generator, revisited. comp.lang.fortran listserv (25 September 2000).

Marsaglia, G., Zaman, A.,1993. The KISS generator. Technical Report, Department of Statistics, Uiversity of Florida.

Mobley, C.D., 1994. Light and Water: Radiative Transfer in Natural Waters. Academic Press, San Diego, CA, (592 pp).

Mobley, C.D., Gentili, B., Gordon, H.R., Jin, Z., Kattawar, G.W., Morel, A., Reinersmam, P., Stamnes, K., Stavn, R.H., 1993. Comparison of numerical models for computing underwater light fields. Applied Optics 32 (36), 7484–7504.

Morel, A., Prieur, L., 1977. Analysis of variations in ocean color. Limnology and Oceanography 22, 709–722.

Petzold, T.J., 1972. Volume Scattering Functions for Selected Ocean Waters. Scripps Institution of Oceanography Ref. 72–78, University of California, San Diego, La Jolla, CA, (79 pp).

Pitcher, T.J., 1993. Behaviour of Teleost Fishes. Chapman & Hall, New York, NY.

Preisendorfer, R.W., 1976. Hydrologic Optics, vol. I: Introduction. US Department of Commerce, Washington, DC, (218 pp).

Sathyendranath, S., Platt, T., 1997. Analytical model of ocean color. Applied Optics 36 (12), 2620–2629.

Stavn, R.H., Weidmann, A.D., 1992. Raman scattering in ocean optics: quantitative assessment of internal radiant emission. Applied Optics 31 (9), 1294–1303.